Polarization screening and induced carrier density at the interface of LaAlO 3 overlayer on SrTiO 3 (001)

Yun Li and Jaejun Yu

Citation: Journal of Applied Physics **108**, 013701 (2010); doi: 10.1063/1.3455877
View online: http://dx.doi.org/10.1063/1.3455877
View Table of Contents: http://scitation.aip.org/content/aip/journal/jap/108/1?ver=pdfcov
Published by the AIP Publishing

Polarization screening and induced carrier density at the interface of $LaAlO_3$ overlayer on $SrTiO_3$ (001)

Yun Li and Jaejun Yu
Department of Physics and Astronomy, FPRD, Center for Strongly Correlated Materials Research, Seoul National University, Seoul 151-747, Republic of Korea

(Received 1 April 2010; accepted 19 May 2010; published online 1 July 2010)

We investigate the role of lattice polarization in determination of induced carrier density at the *n*-type interface of $LaAlO_3$ overlayer on $SrTiO_3$ (001) by carrying out density-functional-theory calculations. When no oxygen vacancy or defect is present, the magnitude of polarization screening in the $LaAlO_3$ layers is found to be correlated with the carrier charge induced at the interface. For the interfaces with less than seven $LaAlO_3$ layers, the density of induced carrier is smaller than 0.1 electrons per unit-cell and the electrostatic screening can be covered by the interface state consisting of Ti d_{xy} state. When the overlayer becomes thicker, the extended bound state in the $SrTiO_3$ side contributes to the charge screening. © *2010 American Institute of Physics*. [doi:10.1063/1.3455877]

I. INTRODUCTION

The observation of a high mobility electron gas in the *n*-type $(LaO)/(TiO_2)$ interface between two band-gap insulators $LaAlO_3$ (LAO) and $SrTiO_3$ (STO) has generated intense research activities toward its potential device applications as well as its physical mechanism.[1] The electronic reconstruction at the interface has been suggested as a way to avoid the polarization catastrophe[2] which may arise from the alternating stack of positively charged LaO and negatively charged AlO_2 layers on top of the TiO_2 termination of STO substrate.

While the reports of ferromagnetism[3] and superconductivity[4] in the LAO/STO interface have boosted up research interest in the mechanism of conductivity and the dimensionality of the induced charge carrier at the interface, there still remain controversies on the origin and nature of the interface electron gas.[5,6] Several experiments have demonstrated that oxygen vacancies in the STO layer are responsible for the high carrier density, which depends more on the film growth and annealing conditions.[7–9] Apart from the oxygen-vacancy-generated carriers in samples grown in oxygen-poor conditions, the carrier density of the *n*-type interfaces with perfect stoichiometry poses another puzzle that a common lower limit in the carrier density at $\sim 10^{13}$, i.e., 0.03 electrons per unit-cell (u.c.), is order-of-magnitude less than that of 0.5 electrons per u.c. expected from the electronic reconstruction mechanism.[10]

On the other hand, recent density-functional-theory (DFT) calculations pointed out the importance of polar distortions as a source of dielectric screening in the LAO/STO heterostructure.[11,12] Without the lattice relaxation, even a single layer of LAO on STO(001) with an ideal structure would become metallic. Further the insulator-to-metal transition can be driven by an external electrical field.[10,13] The thickness dependence of carrier density also suggested a possible role of electrostatic screening in the LAO/STO interface.[14]

Here we show that the detailed balance between the lattice polarization and the charge transfer is important in determination of the carrier density at the *n*-type interface of LAO overlayers on STO(001) with perfect stoichiometry. Our DFT calculations demonstrate that the lattice polarization of the LAO overlayer is correlated with the carrier charge induced at the interface in terms of the overlayer thickness. When the LAO overlayers are over a critical thickness, the charge transfer from the LAO surface to the interface is compensated by the electrostatic screening due to the polarization distortions across the LAO layers.

II. METHOD

We carried out DFT calculations by using the Vienna *ab initio* Simulation Package (VASP) (Ref. 15) within a generalized gradient approximation[16] together with the projector augmented wave pseudopotentials[15,17,18] and the cut-off energy of 400 eV for the plane wave basis. We modeled the LAO/STO interface by a slab consisting of one-to-ten LAO layers on top of seven STO(001) layers and a vacuum region of 14 Å along the *c*-axis in a supercell geometry. Dipole corrections were used to correct the errors of electrostatic potential, forces, and total energy caused by periodic boundary condition.[19] The in-plane unit cell for calculations was taken as (1×1) because the rotation distortion of TiO_6 octahedron is known to be negligible for small carrier doping.[12,20] The in-plane lattice constant of the slab was constrained at the calculated equilibrium lattice constant $a=3.942$ Å of the STO substrate. The *c*-axis coordinates of atomic positions were fully relaxed with forces less than 0.01 eV/Å except for the atoms in the bottom three layers of STO, which were fixed in their bulk structure.

In order to determine accurately the amount and distribution of carrier density as a function of the layer thickness, we had to devise a proper k-point sampling for the LAO/STO slab calculations. For insulating states, the k-point grid of $(12\times12\times1)$ was found to be good enough for the self-consistency iterations. For the case with metallic charge carriers, however, it was required to introduce an extra dense grid set near Γ and *M* points because the accurate evaluation of the tiny pocket sizes of Fermi surfaces is critical for the

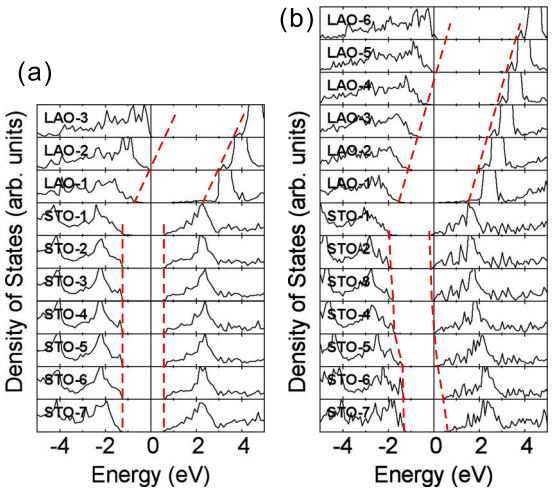

FIG. 1. (Color online) Layer pDOS of (a) $(LAO)_3/(STO)_7$ and (b) $(LAO)_6/(STO)_7$. Dashed lines are drawn by connecting band edges to represent the layer-dependent potential profile.

correct description of the charge carrier as well as the electrostatic potential across the interface. For the dense grid set, we used 0.02 eV as a Gaussian broadening parameter.

III. RESULTS AND DISCUSSION

A. Polarization screening in LAO overlayer

One of the most prominent features in the calculated relaxation geometry of the LAO/STO slab is the presence of a large polar distortion in the LaO and AlO_2 layers but a negligible distortion in the STO side.[12] Because of the huge dipole field produced by the alternating stack of $(LaO)^+$ and $(AlO_2)^-$ charged layers, all the LaO and AlO_2 layers become buckled except the surface AlO_2 layer which exhibits only a small uniform relaxation. The relative displacement between La and O ions within the LaO layers varies from 0.1 to 0.35 Å, depending on the LAO thickness as well as the location of LaO layers, while the relative displacements between Al and O ions within the AlO_2 layers remain less than 0.15 Å.

The screening by the polar distortion is critical in understanding the interface electronic structure. We obtained an interesting relaxation dependence of the LAO/STO interface character in the overlayer structure, which is similar to the results by Pentcheva and Pickett[12] but apparently quite different from that of $(LAO)_m/(STO)_n$ superlattices.[21] Regardless of their thickness, all the *unrelaxed* overlayer structures were found to have a metallic interface. After the relaxation, however, the LAO/STO interface remains insulating up to four layers of LAO. In the systems with one-to-four LAO layers, the lattice polar distortion is favored energetically over the charge transfer between the surface and the interface.

Figure 1 shows the layer-projected density-of-states (pDOS) of two representative systems with fully relaxed LAO layers: (a) $(LAO)_3/(STO)_7$ and (b) $(LAO)_6/(STO)_7$. The pDOS of the relaxed $(LAO)_3/(STO)_7$ exhibits an insulating band structure where the valence band maximum (VBM) of the LAO layers is set at the LAO surface layer. The dipole field in the LAO layers shifts the LAO band edges toward the higher energy relative to those of STO. The potential gradient is about 0.6 eV per layer for the relaxed structure, whereas it would be about 1.3 eV for the unrelaxed structure without polar distortions. It is noted that the VBM of the LAO surface layers, i.e., LAO-3 of Fig. 1(a) and LAO-6 of Fig. 1(b) deviates significantly from the extrapolated (dashed) lines connecting the VBM's of its subsurface layers. The lowering of the VBM of the LAO surface layer is attributed to its local environment being close to the bulk Al_2O_3 with a band gap larger than that of LAO. In addition to the surface effect, there also exists a band offset at the interface. There is a small but clear offset of about 0.5 eV between the LAO-1 and STO-1 layers, while the conduction band minimum (CBM) of the LAO-1 interface layer smears due to the hybridization between LaO and TiO_2 layers.

The band edge shift in the LAO side reflects the change of electrostatic potential across the LAO overlayers. In Fig. 1, the layer-dependent potential profiles are marked by dashed lines. The gradient of the edge shift in (a) $(LAO)_3/(STO)_7$ is higher than that in (b) $(LAO)_6/(STO)_7$. From our calculations, in the system with $m=4$ in $(LAO)_m/(STO)_7$, the VBM of the surface LAO layer barely touches the CBM of the interface STO layer. When we have more than four LAO layers, the LAO/STO interface becomes metallic. As shown in Fig. 1(b) of the pDOS of the relaxed $(LAO)_6/(STO)_7$ structure, the charge carrier at the LAO/STO interface is induced as a result of charge transfer from the LAO surface. Despite that the potential gradient is reduced significantly by the polarization screening, the total potential shift across the LAO layers exceeds the STO band gap when the overlayer thickness goes over a critical value of four LAO layers. If the VBM of the surface LAO layer lies above the CBM of the interface STO layer, a charge transfer can occur between the LAO surface and the LAO/STO interface. From the results, we found that the total shift in the VBM is always delimited by the STO band gap for all $m \geq 4$. It implies that the potential shift is somehow compensated by the charge transfer. The polar distortion occurs in response to a local electric field, i.e., the potential gradient in the LAO layers, which in turn depends on the amount of charge transfer. Therefore, in order to determine the amount of charge transfer, it is necessary to understand the relation between the lattice polarization and the charge transfer.

B. Thickness dependence of lattice polarization

In order to quantify the thickness dependence of the lattice polarization, we calculated the layer-by-layer polarization over the LAO layers as a functional of the LAO layer thickness. Polarization P_ℓ of the ℓ-th layer can be estimated by

$$P_\ell = \frac{1}{\Omega_\ell} \sum_{i \in \ell} Z^*_{\ell i} \delta u_{\ell i}, \tag{1}$$

where $Z^*_{\ell i}$ and $\delta u_{\ell i}$ are the Born effective charge and the displacement of the i-th ion in the ℓ-th layer, respectively, and Ω_ℓ is the volume of the LAO unit cell in the ℓ-th layer. Here we took the values of the Born effective charges from Ref. 22. Since Eq. (1) can be used for the either La or Al

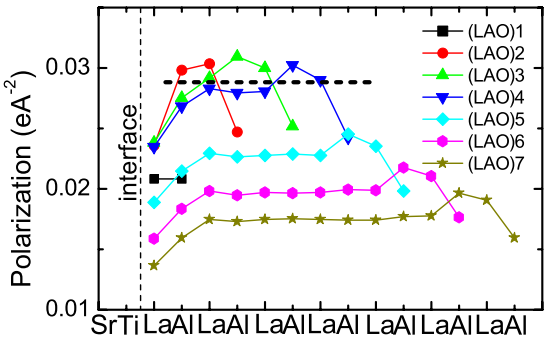

FIG. 2. (Color online) Calculated layer-by-layer polarization P_ℓ over the LAO layers for $(LAO)_m/(STO)_7$ ($m=1\sim7$). Labels "La" and "Al" correspond to the LaO and AlO_2 layers, respectively.

cation-centered cells, we averaged out the contributions of the oxygens in the planes bounding the elementary unit cells.[23]

Figure 2 illustrates the profile of the layer-by-layer polarization P_ℓ over the LAO layers for $(LAO)_m/(STO)_7$ ($m=1\sim7$). In all cases, it is noted that the polarizations of the interface and surface layers are significantly different from their average values. Although a reduction in the interface polarization may arise from both structural relaxation and charge screening, its origin may require a further investigation but is expected to be different from that of the ferroelectric insulator superlattices.[24] Aside from the polarizations at the interface and surface layers, the average values of P_ℓ for $n=2$, 3, and 4, denoted by a dashed line in Fig. 2, are roughly constant at about 0.03 e/Å^2. From $m=4$ to 7, The average value of P_ℓ drops quickly as the layer thickness increases. This decrease in P_ℓ is related to the reduction in the potential gradient in the LAO layers, which is delimited by the STO band gap and the charge transfer between the surface and the interface.

For a given thickness t for $m\geq4$, since the potential shift in the LAO layers is delimited by the STO band gap, the local electric field E_d can be approximated by $E_d=V_g^{STO}/(t-t_0)$ where V_g^{STO} is a potential change corresponding to the STO band gap, and t_0 is an effective parameter corresponding to the dead layer contribution.[25] As the layer polarization P_ℓ is proportional to the local field E_d, the inverse of the average polarization P_ℓ should satisfy the relation

$$\frac{1}{P_\ell}=\frac{1}{\chi\epsilon_0 E_d}=\frac{1}{\chi\epsilon_0 V_g^{STO}}(t-t_0), \tag{2}$$

where χ is an average polarizability of the LAO layers. The t-dependence of P_ℓ in Eq. (2) is clearly demonstrated in the plot of $1/\langle P_\ell\rangle$ versus t as shown in Fig. 3(a). For $m\geq4$, $1/\langle P_\ell\rangle$ increases linearly in t, while it remains constant below $m=4$ except for the $m=1$ case. The deviation of the $m=1$ polarization is not surprising because the single LAO layer consists of both surface and interface layers. From the least square fit to the calculated data, we could determine the effective parameter t_0 by $t_0=0.053c_0$ where c_0 is the u.c. thickness of the LAO layer.

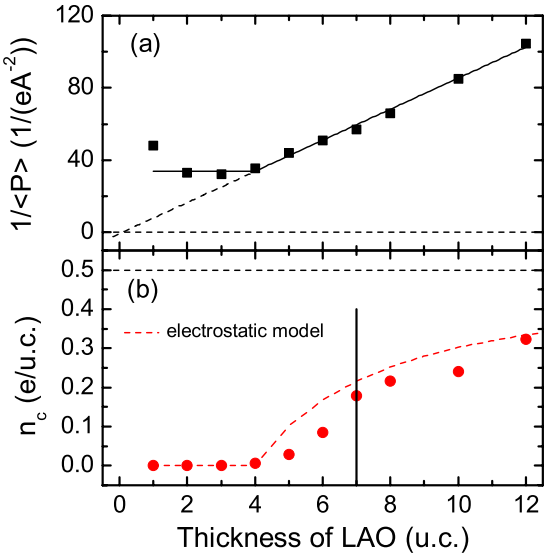

FIG. 3. (Color online) The LAO thickness dependence of (a) the average inverse polarization $1/\langle P_\ell\rangle$ and (b) the charge carrier density n_c.

C. Induced carrier density

For the metallic interface with $m\geq4$, the potential shift, generated by the dipole field arising from the alternating stack of $(LaO)^+$ and $(AlO_2)^-$ charged layers, is screened by both lattice polarization and charge transfer. The relation between the interface (or surface) charge σ_c and the local electric field E_d can be described in a simple electrostatic picture by the electric displacement field across the LAO overlayer: $\sigma_c=\epsilon E_d=\epsilon_0 E_d+P$. If there is no free charge carrier at the interface, an average displacement field should correspond to $\sigma_c=1/2$ as expected from the polarization catastrophe theory.[2] When a charge transfer of n_c occurs, however, the charge screening should give rise to $\sigma_c=1/2-n_c$. By combining the t-dependence of E_d and P_ℓ in Eq. (2), we obtain an expression for the t-dependence of the induced charge carrier n_c at the interface for $m\geq4$

$$n_c=\frac{1}{2}-\frac{A}{t-t_0}, \tag{3}$$

where $A=\epsilon_0(1+\chi)V_g^{STO}$.

The calculated charge carriers density n_c at the LAO/STO are shown in Fig. 3(b). For $m<4$, the insulating interface has no charge carrier. At $m=4$, where the VBM of LAO touches the CBM of STO, the carrier density n_c is $\sim10^{-3}$. For $m>4$, n_c increases monotonically as the thickness of the LAO overlayer grows. For the thin layers with $m<12$, the carrier densities remain far less than 0.5 e/u.c. From Eq. (3), it is obvious that $n_c=0.5$ e/u.c. can be achieved only when the LAO layers become extremely thick. By anchoring the coefficient A to the value of n_c at $m=4$, we obtained $A=1.97$. The fitting result based on the electrostatic model of Eq. (3) is displayed as a dashed line in Fig. 3(b). Despite of some discrepancy for the thin layers close to $m=4$, the electrostatic model is found to be in a reasonable agreement with the DFT results. Considering that the electrostatic model is simplistic and may not be valid in the scale of a few atomic layers, this agreement is rather remarkable.

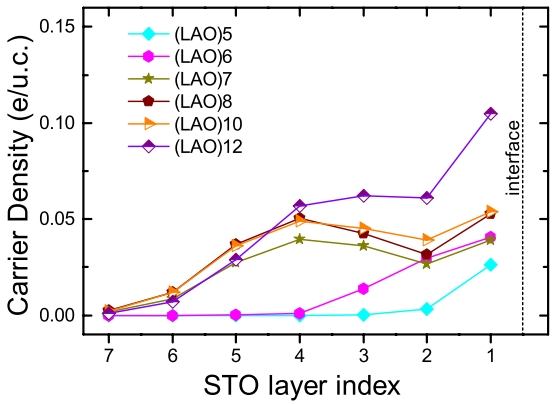

FIG. 4. (Color online) Layer-resolved carrier density in STO for the metallic interface with the varying thickness of LAO overlayer from $m=5$ to 12 in $(LAO)_m/(STO)_7$.

Although our electrostatic model explains the overall behavior of n_c without oxygen vacancy, the induced charge carrier still depends on the detailed electronic structure near the interface. The charge carrier distribution at the interface is closely related to the band bending, i.e., the CBM edge shift in the STO substrate. When there is no charge carrier, i.e., $n_c=0$, for the insulating interface with $m<4$, no band bending occurs in the STO side as shown in Fig. 1(a). For the metallic interface with $m\geq 4$, on the other hand, the degree of the band bending depends on the amount of the charge carrier.

D. Carrier density distribution in STO layers

Figure 4 presents the distribution of layer-resolved carrier density in the STO substrate as a function of the LAO-overlayer thickness m. The carrier densities in the STO side were calculated for the metallic interfaces with $m>4$ in $(LAO)_m/(STO)_7$. The induced carriers for $m=5$ and 6 are confined within three STO layers adjacent to the LAO/STO interface, while the carrier densities for $m\geq 7$ are more extended away from the interface. The confinement of the carrier for $m=5$ and 6 is consistent with a recent x-ray photoelectron spectroscopy (XPS) experiment, which reported that the carriers far less than 0.5 e/u.c. are confined in one or a few layers of STO for thin LAO film without oxygen vacancy.[26]

Depending on the overlayer thickness m, however, there are two components contributing to the carrier distribution: a tail residing close to the LAO/STO interface and a bump centered near the fourth STO layer as shown in Fig. 4. While the tail component exists regardless of the LAO thickness, i.e., the magnitude of the charge carrier, the broad bump appears only for $m\geq 7$. It implies that the interface-related state is enough to cover the induced charge carrier when the carrier density is less than 0.1, i.e., for $m=5$ and 6. On the other hand, when the amount of induced carrier density exceeds 0.1, i.e., for $m\geq 7$, it is necessary to have additional contribution from the extended state away from the interface. As the LAO overlayer becomes thicker than $m=7$, the weight of the induced charge carrier shifts drastically from the tail component to the broad bump.

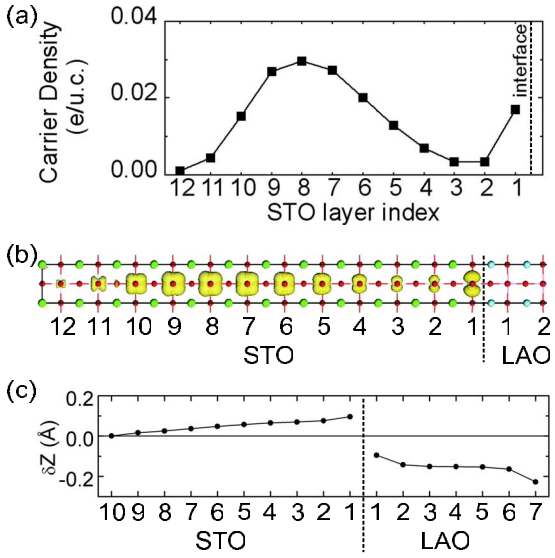

FIG. 5. (Color online) (a) Layer-resolved carrier densities in STO for $(LAO)_7/(STO)_{12}$. (b) Charge density plot of the induced carrier for $(LAO)_7/(STO)_{12}$. (c) Polar distortions in the LaO and SrO layers represented by the relative displacements between anion (O) and cation (La or Sr), i.e., $\delta z=z_O-z_{La,Sr}$.

The profile of the bump structure in Fig. 4 suggests that the bump is related to the long range screening potential, i.e., the band bending in the STO side. However, the calculated curves of the carrier density for $m\geq 7$ seem to be limited by the STO thickness. Although seven layers for the STO substrate were found to be enough for the description of the LAO overlayer, the proper description of the induced carrier in the STO side needs even thicker STO layers. In order to probe the physical characteristics of the induced charge carrier in the STO side, we carried out the calculations of the induced carrier for $(LAO)_7/(STO)_{12}$ by employing 12 STO layers. The calculated carrier distribution in $(LAO)_7/(STO)_{12}$ demonstrates a clear separation of the interface component and the bump component, as illustrated in Fig. 5(a). While the interface component is confined close to the interface layer, the bump component extends further into the STO substrate and has a broad peak near the eighth layer, i.e., about 3 nm from the interface. The potential profile visualized by the band bending in the STO side of Fig. 1(b) resembles the case of the inversion layer in metal-oxide-semiconductor field-effect transistor and semiconductor heterostructures.[27] There is a finite barrier at the LAO side and a gradual change toward the bottom of the STO substrate. In this potential, the bound states described by the Airy function may lead to a charge accumulation at a few nm away from the interface.[27] Despite that the separation of the interface and bump contributions in the case of $(STO)_{12}$ is much more pronounced than that of $(STO)_7$ in Fig. 4, the difference in the total induced charge n_c between $(STO)_7$ and $(STO)_{12}$ is rather minimal being close to 0.01.

To understand the nature of two different contributions in the induced charge carrier, we plotted the charge density of the induced carrier in the STO side of $(LAO)_7/(STO)_{12}$ in Fig. 5(b). The interface component consists mostly of the Ti d_{xy} orbitals, but the bump component has contributions from all the Ti t_{2g} orbitals, i.e., d_{xy}, d_{yz}, and d_{zx} states. The

different character at the interface stems from a strong compressive distortion of the TiO_6 octahedron at the interface. The distortions of neighboring La–O and Sr–O layers toward the interface TiO_2 layer causes a compression of the TiO_6 octahedron along the z direction, which produces a strong tetragonal field leading to a lowering of the d_{xy} state. Figure 5(c) shows the polar displacements in the LaO and SrO layers. It is noted that the lattice polarization in the STO side is opposite to that in the LAO overlayer. When $n_c \approx 0$, the lattice distortion in the STO side is negligible, though it becomes significant as n_c increases.

IV. CONCLUSION

In conclusion, we explored a microscopic picture for the screening mechanism at the interface of the LAO overlayer on STO(001) by carrying out the DFT calculations, and demonstrated that the lattice polarization of the LAO layers is correlated with the carrier charge induced at the interface in terms of the overlayer thickness. Here we suggest an electrostatic model for the description of the charge carrier induced at the interface, where the detailed balance between the lattice polarization and the charge transfer plays a primary role when no oxygen vacancy or defect is present in the system. From the profile of layer-resolved carrier density in the STO side, it is identified that there are two distinct contributions to the induced carrier. When the carrier density is smaller than 0.1 per u.c., the interface state alone can cover the electrostatic screening. Otherwise the extended state related to the STO band bending contributes to the screening process. In this picture, it is natural to observe a common lower limit of 0.03 electrons per u.c. for the systems with four-to-five LAO layers. In addition, one can consider the induced carrier density controlled by an external field, which affect the lattice polarization over the LAO layers.

Although our discussion is restricted to the perfect lattice without defect, the electrostatic screening mechanism across the LAO overlayer should be considered as an alternative to the electronic reconstruction mechanism. Our model calculations predict a metallic LAO surface accompanying the metallic interface in the ideal configuration. In reality, however, there exist oxygen vacancies at the LAO overlayer and the intermixing at the interface, which complicate the interpretation of the surface and interface behavior. A recent x-ray photoemission study[28] reported the absence of an electric field or band bending in the LAO layer, which is not consistent with the polarization catastrophe model. In addition, the intermixing of La and Sr at the LAO/STO interface[2,29] and some amount of oxygen vacancies in the LAO surface[13] were suggested as a possible source of the cancellation of the polar electric field in thin LAO film. Although we have carried out extensive calculations for the effect of oxygen vacancy,[30] still further investigations are required to gain a full understanding of the interface electronic structure. We hope that our findings contribute to resolving the controversies on the origin and nature of the interface electron gas.

ACKNOWLEDGMENTS

This work was supported by the National Research Foundation of Korea through the ARP (R17-2008-033-01000-0) and by the BK21 program. We also acknowledge the support from KISTI under the Supercomputing Application Support Program.

[1] A. Ohtomo and H. Y. Hwang, Nature (London) **427**, 423 (2004).
[2] N. Nakagawa, H. Y. Hwang, and D. A. Muller, Nature Mater. **5**, 204 (2006).
[3] A. Brinkman, M. Huijben, M. Van Zalk, J. Huijben, U. Zeitler, J. C. Maan, W. G. Van Der Wiel, G. Rijnders, D. H. A. Blank, and H. Hilgenkamp, Nature Mater. **6**, 493 (2007).
[4] N. Reyren, S. Thiel, A. D. Caviglia, L. Fitting Kourkoutis, G. Hammerl, C. Richter, C. W. Schneider, T. Kopp, A.-S. Rütschi, D. Jaccard, M. Gabay, D. A. Muller, J.-M. Triscone, and J. Mannhart, Science **317**, 1196 (2007).
[5] M. Basletic, J.-L. Maurice, C. Carrétéro, G. Herranz, O. Copie, M. Bibes, É. Jacquet, K. Bouzehouane, S. Fusil, and A. Barthélémy, Nature Mater. **7**, 621 (2008).
[6] K. Yoshimatsu, R. Yasuhara, H. Kumigashira, and M. Oshima, Phys. Rev. Lett. **101**, 026802 (2008).
[7] A. Kalabukhov, R. Gunnarsson, J. Börjesson, E. Olsson, T. Claeson, and D. Winkler, Phys. Rev. B **75**, 121404(R) (2007).
[8] G. Herranz, M. Basletić, M. Bibes, C. Carrétéro, E. Tafra, E. Jacquet, K. Bouzehouane, C. Deranolt, A. Hamzić, J.-M. Broto, A. Barthélémy, and A. Fert, Phys. Rev. Lett. **98**, 216803 (2007).
[9] W. Siemons, G. Koster, H. Yamamoto, W. A. Harrison, G. Lucovsky, T. H. Geballe, D. H. A. Blank, and M. R. Beasley, Phys. Rev. Lett. **98**, 196802 (2007).
[10] S. Thiel, G. Hammerl, A. Schmehl, C. W. Schneider, and J. Mannhart, Science **313**, 1942 (2006).
[11] S. Ishibashi and K. Terakura, J. Phys. Soc. Jpn. **77**, 104706 (2008).
[12] R. Pentcheva and W. E. Pickett, Phys. Rev. Lett. **102**, 107602 (2009).
[13] C. Cen, S. Thiel, G. Hammerl, C. W. Schneider, K. E. Andersen, C. S. Hellberg, J. Mannhart, and J. Levy, Nature Mater. **7**, 298 (2008).
[14] M. Huijben, G. Rijnders, D. H. A. Blank, S. Bals, S. Van Aert, J. Verbeeck, G. Van Tendeloo, A. Brinkman, and H. Hilgenkamp, Nature Mater. **5**, 556 (2006).
[15] G. Kresse and J. Furthmüller, Phys. Rev. B **54**, 11169 (1996).
[16] Y. Wang and J. P. Perdew, Phys. Rev. B **44**, 13298 (1991).
[17] P. E. Blöchl, Phys. Rev. B **50**, 17953 (1994).
[18] G. Kresse and D. Joubert, Phys. Rev. B **59**, 1758 (1999).
[19] G. Makov and M. C. Payne, Phys. Rev. B **51**, 4014 (1995).
[20] K. Uchida and S. Tsuneyuki, Phys. Rev. B **68**, 174107 (2003).
[21] K. Janicka, J. P. Velev, and E. Y. Tsymbal, Phys. Rev. Lett. **102**, 106803 (2009).
[22] S. Gemming and G. Seifert, Acta Mater. **54**, 4299 (2006).
[23] S. M. Nakhmanson, K. M. Rabe, and D. Vanderbilt, Appl. Phys. Lett. **87**, 102906 (2005).
[24] J. H. Lee, J. Yu, and U. Waghmare, J. Appl. Phys. **105**, 016104 (2009).
[25] M. Stengel and N. A. Spaldin, Nature (London) **443**, 679 (2006).
[26] M. Sing, G. Berner, K. Goß, A. Müller, A. Ruff, A. Wetscherek, S. Thiel, J. Mannhart, S. A. Pauli, C. W. Schneider, P. R. Willmott, M. Gorgoi, F. Schäfers, and R. Claessen, Phys. Rev. Lett. **102**, 176805 (2009).
[27] T. Ando, A. B. Fowler, and F. Stern, Rev. Mod. Phys. **54**, 437 (1982).
[28] Y. Segal, J. H. Ngai, J. W. Reiner, F. J. Walker, and C. H. Ahn, Phys. Rev. B **80**, 241107(R) (2009).
[29] A. S. Kalabukhov, Y. A. Boikov, I. T. Serenkov, V. I. Sakharov, V. N. Popok, R. Gunnarsson, J. Börjesson, N. Ljustina, E. Olsson, D. Winkler, and T. Claeson, Phys. Rev. Lett. **103**, 146101 (2009).
[30] Y. Li, S. Na-Phattalung, S. Limpijumnong, J. Kim, and J. Yu (unpublished).